# Size-quantized oscillations of the electron mobility limited by the optical and confined acoustic phonons in the nanoscale heterostructures

E. P. Pokatilov and D. L. Nika
*Nano-Device Laboratory, Department of Electrical Engineering, University of California—Riverside, Riverside, California 92521, USA*

A. S. Askerov
*Department of Theoretical Physics, State University of Moldova, MD-2004 Kishinev, Moldova*

A. A. Balandin[a)]
*Nano-Device Laboratory, Department of Electrical Engineering, University of California—Riverside, Riverside, California 92521, USA*

(Received 30 May 2007; accepted 16 July 2007; published online 7 September 2007)

The authors theoretically investigated the electron mobility in the nanometer thickness AlN/GaN/AlN heterostructures limited by the polar optical and confined acoustic phonons. The proposed model accurately takes into account dispersion of the optical and acoustic phonons in such heterostructures as well as inelasticity of the electron scattering on both optical and acoustic phonons. It has been shown that the intersubband electronic transitions play an important role in limiting the electron mobility when the energy separation between one of the size-quantized excited electron subbands and the Fermi energy becomes comparable to the optical or confined acoustic phonon energy. The latter results in the nonmonotonic oscillatory dependence of the electron mobility on the thickness of the GaN conduction channel layer. The predicted effect is observable at room temperature and over a wide range of carrier densities. The described mechanism can be used for fine tuning the confined electron and phonon states in the nanoscale heterostructures made of different material systems in order to achieve performance enhancement of the nanoscale electronic devices. © *2007 American Institute of Physics*. [DOI: 10.1063/1.2777105]

## I. INTRODUCTION

The optical and acoustic phonons play a major role in limiting the electron mobility near the room temperature.[1] Depending on the type of a semiconductor, e.g., nonpolar or polar, and temperature, the relative contribution of the optical and acoustic phonons to the electron-phonon scattering can differ over a wide range. The electron-phonon scattering rates can undergo strong modification in the hetero- and nanostructures with the size-quantized electronic states. Lee and Vassell[2] have shown that the low-field drift electron mobility in the thin quantum wells or narrow conduction channels decreases below the bulk limit due to the electron state size quantization. At the same time, there exists an intermediate range of the quantum well thicknesses where the carrier mobility is enhanced. Their calculation was carried out in the relaxation time approximation for a single electron band and bulk acoustic and optical phonons. The methods of enhancing the carrier mobility via tuning the size-quantized electron states became an important part of the electron band–structure engineering.[1]

More recently, Fonoberov and Balandin[3] found that the low-field room temperature electron mobility in silicon nanowires with the barriers made of the "acoustically hard" materials can be increased via partial suppression of the deformation potential electron–acoustic phonon scattering. The results were obtained for the nanowires with the size-quantized electron states and confined acoustic phonon dispersion, which was modified due to the elastic mismatch at the interface between the nanowire and the barrier materials. In another material system the low-temperature electron mobility was found to undergo changes due to the mismatch between the acoustic phonon density of states (PDOS) in the dissimilar nanowire and barrier materials.[4] The methods for the electron mobility enhancement via the controlled modification of the phonon dispersion became a part of what is now referred to as phonon engineering.[5]

It was previously shown both theoretically and experimentally that the carrier mobility can manifest a nonmonotonic dependence on the thickness of the conduction channel.[6–11] The theoretical treatment of Inoue and Matsuno,[6] which analyzed the mobility dependence on the channel thickness in AlGaAs/GaAs/AlGaAs system, was based on the system of two Boltzman equations and included the major mechanisms of the electron scattering, e.g., charge impurities, lattice defects, and phonons. The electron scattering on the acoustic phonons was approximated as an elastic process, while the nonelasticity of the electron scattering on optical phonons was explicitly taken into account. Tsuchia and Ando[7] have considered a similar problem for AlAs/GaAs/AlAs material system but introduced a more complicated confining potential profile.

In this paper, we examine the dependence of the electron mobility on the conduction channel thickness in AlN/GaN/AlN heterostructure using a rigorous theoretical

a)Author to whom correspondence should be addressed. Electronic mail: balandin@ee.ucr.edu. URL: http://www.ndl.ee.ucr.edu/

 © 2007 American Institute of Physics

Downloaded 12 Oct 2007 to 138.23.166.189. Redistribution subject to AIP license or copyright, see http://jap.aip.org/jap/copyright.jsp

approach. Specifically, our model takes into account the (i) multiple size-quantized electron subbands, (ii) dispersion of the optical and acoustic phonons in such structure, as well as (iii) inelasticity of electron scattering on both optical and acoustic phonons. It is well known that GaN and AlN can form both wurtzite and zinc-blende crystal structure. The electron mobility in wurtzite AlN/GaN/AlN structures is strongly affected by the built-in electric field due to the spontaneous and piezoelectric polarization.[12,13] To separate the effect due to the built-in field from the nanoscale size quantization and phonon dispersion effects, we considered the zinc-blende AlN/GaN/AlN system. The AlN/GaN/AlN heterostructures present a particularly interesting case for the study of the mobility dependence on the channel thickness due to the high energy of the optical phonons in these materials (66–100 meV range), which allows one to elucidate the origin of the nonmonotonic dependence.

The remainder of the paper is organized as follows. In the next section, we describe the theoretical model based on the system of the Boltzman kinetic equations and the calculation procedure. Section III presents our results and comparison with the available experimental data. The conclusions are given in Sec. IV.

## II. THEORETICAL MODEL AND CALCULATION PROCEDURE

For many technologically important semiconductors the energies of the optical phonons are similar to the energies of the acoustic phonons, which correspond to the Debye cutoff frequency. For example, in GaAs, the energy of the optical phonon is $\hbar\omega_{\mathrm{opt}}=36$ meV, while the Debye acoustic phonon energy is $\hbar\omega_{\mathrm{ac}}=30$ meV. The optical phonon energies in the zinc-blende and wurtzite GaN are 87 and 91 meV, respectively. The energies of the acoustic phonons, which correspond to the Debye cutoff frequencies, are around 50 meV.[14] Thus, it is important to take into account the inelasticity of the electron interaction with both optical and acoustic phonons in the calculation of the phonon-limited mobility. The phonon dispersion is also explicitly taken into account in our theoretical model and calculation procedure. The latter is particularly important for the acoustic phonon dispersion, which undergoes modification in the nanometer thickness heterostructures.

The nonmonotonic dependence of the electron mobility on the channel thickness $d$, i.e., oscillatory behavior, can appear owing to various reasons. One can envision a "quasiresonant" condition when the electron scatters from the populated low-energy subband into the unoccupied higher-energy subband with the absorption of a phonon with suitable energy and momentum. In this case, the Fermi energy is considerably lower than the energy of the higher subband but the energy of the phonon is enough for the electron transition to take place. The elastic scattering processes do not contribute to such scattering transitions. Completely different situation develops when the Fermi level is close to the energy of one of the higher-energy subbands, which is partially populated. The latter may happen when the channel thickness $d$ increases (while still in the size-quantized limit) leading to the small energy separations between the subbands. The elastic (or quasielastic) electron transitions can contribute to the electron scattering in this case. The physical mechanism behind the observed mobility maxima in GaAs-based heterostructures[6] was likely related to the Fermi energy alignment with the first excited subband and contribution of the elastic scattering processes.

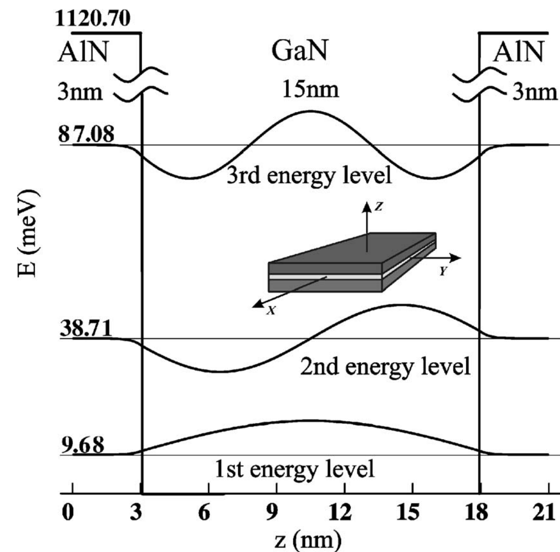


FIG. 1. Electron energy levels and wave functions for the ground ($n=1$) and excited ($n=2$ and 3) subbands in the zinc-blende AlN/GaN/AlN heterostructure with the dimensions of 3 nm/15 nm/3 nm. The inset shows the heterostructure geometry and the coordinate system.

The procedure for calculating the electron mobility in semiconductor nano- or heterostructures is different, depending on the conduction channel thickness. If the channel layer is relatively thick one can use the "bulk" approach assuming that there are no spatial confinement effects for either electrons or phonons and neglect the interaction between the electrons and interface phonons. Such approach has been used in the calculation of the electron mobility in the modulation-doped structures and some device heterostructures.[1] When the channel is very thin (on the order of the electron de Broglie wavelength or smaller) the electron size quantization has to be taken into account. Commonly, in such cases, it was assumed that only the ground electron subband is occupied and the intersubband electron transitions were omitted.[15,16] However, in heterostructures with the nanometer scale thickness of the conduction channels ($d\sim 5$ nm for zinc-blende AlN/GaN/AlN heterostructures), the energy separation between the quantized electron levels $\Delta\varepsilon_{n,n-1}=\varepsilon_n^0-\varepsilon_{n-1}^0$ ($\varepsilon_n^0$ is the energy of $n$th quantized level) is comparable to the phonon energy. For this reason the intersubband electron transitions should be taken into consideration. One should note here that this case is the most relevant to the realistic electronic devices structures made of AlN/GaN/AlN.

We calculate the electron mobility for the zinc-blende AlN/GaN/AlN heterostructures with the flat potential in the bottom of the conduction band (see inset of Fig. 1 for the heterostructure geometry). For the GaN conduction channels with the thicknesses $d=2-22$ nm the three lowest electron subbands participate in the intrasubband electron scattering

Downloaded 12 Oct 2007 to 138.23.166.189. Redistribution subject to AIP license or copyright, see http://jap.aip.org/jap/copyright.jsp

transitions. The electron relaxation times can be found from the solution of a system of the integral-differential Boltzman kinetic equations written as,[13,17]

$$\sum_{\substack{\mathbf{p}',m=\pm 1,\\ \lambda,n'=1,2,3}} \left\{ W(n,\mathbf{p}\rightarrow n',\mathbf{p}')\frac{1-f^0[\varepsilon_n+m\hbar\omega_\lambda(q)]}{1-f^0(\varepsilon_n)} \times\left[\tau_n(\mathbf{p})-\tau_{n'}(\mathbf{p}')\frac{\mathbf{pp}'}{p^2}\right]\right\}=1, \quad (1)$$

where $W(\gamma\rightarrow\gamma')=(2\pi/\hbar)|<\gamma|\hat{H}_{e-\mathrm{ph}}|\gamma'>|^2\delta(E_\gamma-E_{\gamma'})$ is the probability of a transition of the electron-phonon system from the state $\gamma$ with the energy $E_\gamma$ to the state $\gamma'$ with the energy $E_{\gamma'}$, $f^0(\varepsilon)=(\exp[(\varepsilon-\varepsilon_F)/k_BT]+1)^{-1}$ is the Fermi-Dirac equilibrium distribution function, $T$ is the absolute temperature, $k_B$ is Boltzman's constant, $\varepsilon$ is the electron energy, $q$ is the phonon wave number, $\mathbf{p}$ and $\mathbf{p}'$ are the electron momenta in the initial and final states, respectively, $\lambda$ is the quantum number of the polar optical (interface or confined) or acoustic phonon modes, $\hat{H}_{e-\mathrm{ph}}$ is the Hamiltonian of the electron interaction with the optical or acoustic phonon normal modes, $\tau_1(\varepsilon)$ is the kinetic relaxation time of an electron with the energy $\varepsilon$ in the ground subband, which includes the transitions $(1\leftarrow\rightarrow 1)$, $(1\rightarrow 2)$, and $(1\rightarrow 3)$, $\tau_2(\varepsilon)$ is the kinetic relaxation time of an electron in the second subband, which includes the transitions $(2\rightarrow 1)$, $(2\leftarrow\rightarrow 2)$, and $(2\rightarrow 3)$, and $\tau_3(\varepsilon)$ is the electron kinetic relaxation time in the third subband, which includes the transitions $(3\rightarrow 1)$, $(3\rightarrow 2)$, and $(3\leftarrow\rightarrow 3)$, and the indices $n=1$, 2, and 3. The notation $(1\leftarrow\rightarrow 1)$ means transitions within the first electron subband ($n=1$ and $n'=1$); the notation $(1\rightarrow 2)$ means transitions from the first to the second electron subband ($n=1$ and $n'=2$); the rest of the notations are analogous.

The calculation of the electron mobility through the kinetic relaxation times, determined from Eq. (1), is more accurate than the conventionally used relaxation time approximation.[1] After the kinetic relaxation times were determined, we calculated the electron mobility by extending the standard formalism[18] to include the intersubband and intrasubband transitions in the excited subbands ($n=n'=2,3$), which led to the expression

$$\mu(T)=\frac{e}{k_BT}\frac{\sum_{n=1}^{3}\frac{1}{\bar{m}}\int_0^\infty \varepsilon\tau_n(\varepsilon)f^0(\varepsilon)[1-f^0(\varepsilon)]d\varepsilon}{\sum_{n=1}^{3}\int_0^\infty f^0(\varepsilon_n^0+\varepsilon)d\varepsilon}, \quad (2)$$

where $e$ is the electron charge, and $\bar{m}_n$ is the effective electron mass averaged with the electron wave functions for the $n$th energy level calculated by taking into account the electron penetration in the barrier layers.[19] The averaging procedure is needed in order to account for the finite wave function penetration to the barriers and the difference in the electron effective masses in the channel layer and the barriers.

The evaluation of the transition matrix elements in Eq. (1) requires the knowledge of the size-quantized electron wave functions for the heterostructure potential with the finite barrier height. We obtained the electron wave functions from the numerical solutions of the Schrödinger equation. Figure 1 shows the electron wave functions $\varphi_n(z)$ and quantized energies $\varepsilon_n^0$ for the ground ($n=1$) and two excited ($n=2$ and 3) electron subbands in the AlN/GaN/AlN heterostructure. The electron in the ground state subband strongly interacts with the confined optical phonons and weakly interacts with the interface optical phonons since the electron is localized in the center of the GaN channel. The intrasubband transitions $(1\leftarrow\rightarrow 1)$, $(2\leftarrow\rightarrow 2)$, and $(3\leftarrow\rightarrow 3)$ and the intersubband transitions $(1\leftarrow\rightarrow 3)$ are governed by the electron interactions with the even-number phonon modes, while the intersubband transitions $(1\leftarrow\rightarrow 2)$ are mediated by the odd-number phonon modes. The latter follows from the symmetry of the electron wave functions and the phonon vibration modes. In the electron ground state and the second excited state the wave functions are antisymmetric with respect to the reflection from the horizontal plane in the center of the channel. The matrix elements of the electron-phonon interaction are nonzero when the product of the complex conjugated wave functions of the initial and final electron states has the same symmetry as the phonon mode, which induces the transition.

While the energies of the optical phonons in AlN/GaN/AlN heterostructures can be taken from literature, one needs to determine the highly dispersive confined acoustic phonon energies for the given heterostructure dimensions and boundary conditions. We accomplish this task by solving the equation of motion for the elastic vibrations in the anisotropic medium, which is written as

$$\rho\frac{\partial^2 U_m}{\partial t^2}=\frac{\partial\sigma_{mi}}{\partial x_i}, \quad (3)$$

where $\mathbf{U}(U_1,U_2,U_3)$ is the displacement vector, $\rho$ is the mass density of the material, $\sigma_{mi}$ is the elastic stress tensor given by $\sigma_{mi}=c_{mikj}U_{kj}$, and $U_{kj}=1/2(\partial U_k/\partial x_j+\partial U_j/\partial x_k)$ is the strain tensor. The details of the solution and simulation procedure for obtaining the confined acoustic phonon modes in three-layered heterostructures were reported by us elsewhere.[20]

## III. RESULTS AND DISCUSSION

After the size-quantized electron states were found, we calculated the energy separation between the confined states and the Fermi level as a function of the conduction channel thickness. The Fermi level position is determined by the selected electron density. The energy separation $\Delta_{nF}(d,N_s)=\varepsilon_n^0-\varepsilon_F$ for the electron subbands $n=2$ and 3 is shown as a function of the channel thickness $d$ in Fig. 2. The maximum ($\hbar\omega_{\max}\sim 110$ meV) and minimum ($\hbar\omega_{\min}\sim 66$ meV) energies of the interface and confined optical phonons in the considered heterostructures are indicated in Fig. 2 with the straight horizontal lines. The material parameters used in our calculation were taken from Refs. 21–23 (see Table I). The intersections of $\Delta_{nF}(d,N_s)$ curves with the maximum and minimum phonon energies $\hbar\omega_{\max,\min}$, given by the expressions $\Delta_{nF}[d_n^0(\mathrm{upper},\mathrm{lower}),N_s]-\hbar\omega_{\max,\min}=0$, are marked with the circles, $d_n^0(u)$ are the channel thicknesses when the

Downloaded 12 Oct 2007 to 138.23.166.189. Redistribution subject to AIP license or copyright, see http://jap.aip.org/jap/copyright.jsp

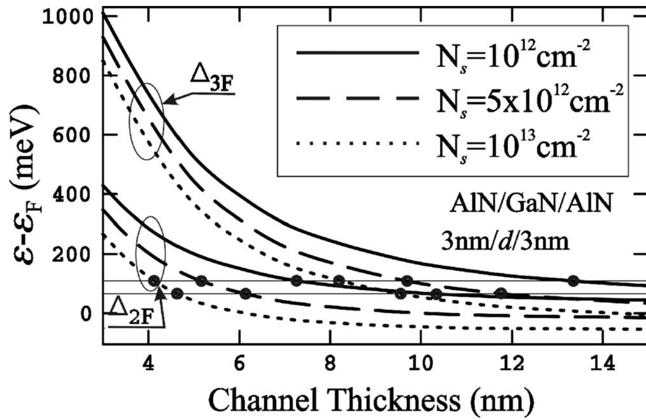


FIG. 2. Subband energy separation from the Fermi level $\Delta_{nF}(d,N_s)=\varepsilon_n^0-\varepsilon_F$ as a function of the conduction channel thickness in AlN/GaN/AlN heterostructure. The results are shown for the excited subbands with $n=2$ and 3. The maximum and minimum energies of the optical phonons are shown with the straight horizontal lines.

upper horizontal line $E=\hbar\omega_{\max}$ intersects with $\Delta_{nF}$ curves, and $d_n^0(l)$ are the channel thicknesses when the lower horizontal line $E=\hbar\omega_{\min}$ intersects with $\Delta_{nF}$ curves (here $u$ denotes "upper" while $l$ denotes "lower"). As it will become clear from the following discussion, these intersections establish approximately the values of the channel thickness when the electron mobility reaches its maximum values for different carrier densities.

Figures 3(a) and 3(b) present the mobility dependence on the channel thickness $d$ for several electron sheet densities $N_s$. The results are shown for the temperature $T=300$ K. The solid, dashed, and dashed-dotted lines in Fig. 3(a) correspond to the electron mobility calculated by taking into account three ($n=1$, 2, and 3), two ($n=1$ and 2), and one ($n=1$) electron subbands, respectively. The electron mobility calculated by including only the intrasubband transitions ($1\leftarrow\rightarrow 1$) increases monotonically with the increasing channel thickness $d$. This dependence agrees with the result obtained by Anderson *et al.*[16] The monotonic increase in the mobility is explained by the fact that the density of the size-quantized electron wave function $|\varphi_n(z,d)|^2$ decreases with the increasing $d$, which leads to the reduction of the matrix elements for the electron—optical phonon interaction. In addition, the interaction between the electron and interface optical phonons also weakens with the increasing thickness of the GaN channel layer. Obviously, the one-subband model calculation can only be considered valid for very thin channels ($d<5$ nm for the given structure) when the subband separation is large (more than a few $k_BT$).

TABLE I. Material parameters for zinc-blende GaN and AlN.

| Material parameters | GaN | AlN |
|---|---|---|
| $\nu_{LO}$ (cm$^{-1}$) | 748[a] | 916[b] |
| $\nu_{TO}$ (cm$^{-1}$) | 562[a] | 673[b] |
| $C_{11}$ (GPa) | 293[c] | 304[c] |
| $C_{12}$ (GPa) | 159[c] | 160[c] |
| $C_{44}$ (GPa) | 155[c] | 193[c] |

[a]Reference 21.
[b]Reference 22.
[c]Reference 23.

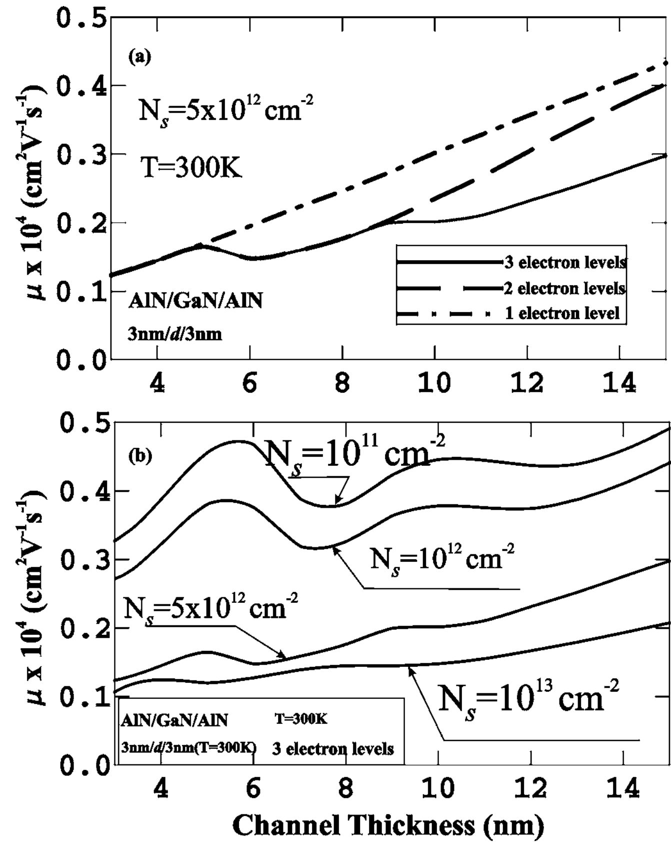


FIG. 3. Room temperature electron mobility limited by the optical and confined acoustic phonons as a function of the conduction channel thickness for (a) different number of electron subband included in the model and (b) different values of the electron sheet concentration.

The electron scattering with the optical phonon accompanied by the optical phonon absorption and electron transition to the excited subbands starts when the phonon energy is somewhat smaller than the energy difference $\Delta_{nF}(d,N_s)$, i.e., already at $d<d_n^0(u,N_s)$, owing to the partial populating of the electron states above the Fermi level. The onset of the intersubband transitions limits the mobility increase even for $d\leqslant d_n^0(u,N_s)$ when the relatively small part of the electrons undergoes the intersubband transitions. Figure 3(b) shows the electron mobility as a function of the channel thickness for several values of the electron concentration. One can see that the mobility attains its maximum value at $d(N_s=10^{13}$ cm$^{-2})=3.8$ nm$<d_2^0(u,N_s=10^{13}$ cm$^{-2})=4.2$ nm, $d(N_s=5\times10^{12}$ cm$^{-2})=4.8$ nm$<d_2^0(u,N_s=5\times10^{12}$ cm$^{-2})=5.2$ nm, and $d(N_s=10^{12}$ cm$^{2})=5.5$ nm$<d_2^0(u,N_s=5\times10^{12}$ cm$^{-2})=7.1$ nm. For the lower electron concentrations ($N_s=5\times10^{12}$ and $10^{12}$ cm$^{-2}$), the onset of the intersubband electron transitions appears at the larger thickness $d$ due to the lager values of $\Delta_{nF}(d,N_s)$.

The intrasubband transitions within the first excited subband actively participate in the electron scattering processes and suppress the mobility oscillations. When $d$ approaches $d_2^0(l,N_s)$ all phonon modes became involved in the electron scattering. At this point, the scattering intensity saturates, and the mobility reaches its minimum value at $d\approx d_2^0(l,N_s)$. The electron transitions to the second excited subband $n=3$ start when the thickness $d$ is still smaller than the critical value

Downloaded 12 Oct 2007 to 138.23.166.189. Redistribution subject to AIP license or copyright, see http://jap.aip.org/jap/copyright.jsp

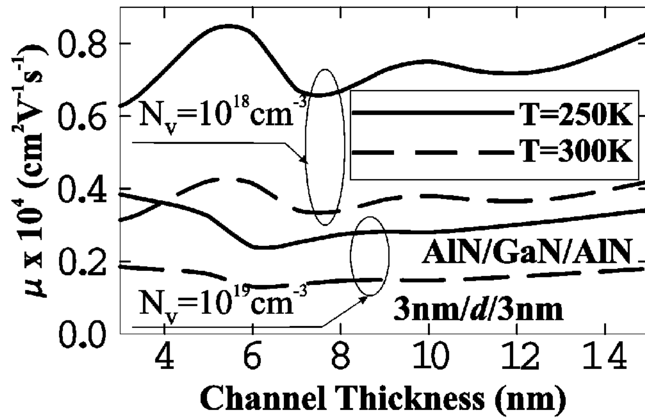


FIG. 4. Room temperature electron mobility limited by the optical and confined acoustic phonons as a function of the conduction channel thickness for two different values of temperature and two values of the electron volumetric concentration.

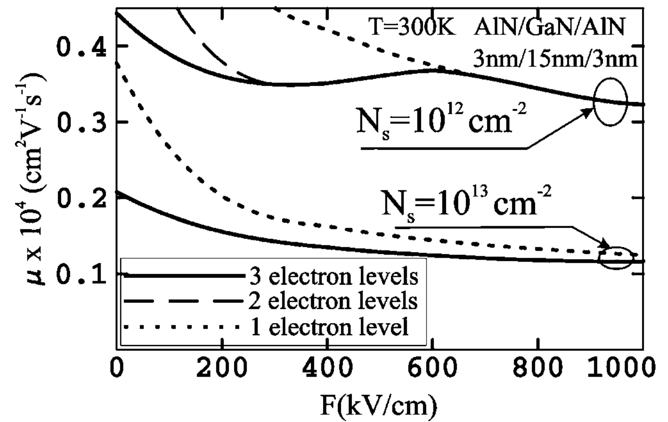


FIG. 5. Electron mobility limited by the optical and confined acoustic phonons as a function of the electric field intensity shown for two different values of the electron sheet density. The electric field is assumed to be perpendicular to the AlN/GaN/AlN heterostructure layers. The solid, dashed, and dotted curves correspond to the mobility calculated by taking into account all three subbands, two subbands, and the ground state subband only.

determined by the intersection in Fig. 1, i.e., $d < d_3^0(u, N_s)$. For the electron concentration $n_s = 10^{12}$ cm$^{-2}$ these transitions appear at $d \approx 9$ nm $< d_3^0(u, N_s = 10^{12}$ cm$^{-2}) = 13$ nm. The slopes of the $\Delta_{3F}$ curves at the points of their intersection with the horizontal "phonon" lines at $d = d_3^0(u, N_s)$ are smaller than the slopes of the $\Delta_{2F}$ curves at the points of their intersection at $d = d_2^0(u, N_s)$. This means that the second maximum and second minimum of the mobility curves are separated by the wider thickness $d$ interval than that for the first ones. The difference between the maximum and minimum mobility values for the second oscillation $\mu_{\max} - \mu_{\min}$ is much smaller than the difference $\mu_{\max} - \mu_{\min}$ for the first oscillation, i.e., $(\mu_{\max} - \mu_{\min}) / \mu_{\min}|_{n=2} = 0.3$ and $(\mu_{\max} - \mu_{\min}) / \mu_{\min}|_{n=3} = 0.027$ for $N_s = 10^{12}$ cm$^{-2}$. The latter is explained by the participation of the ground and first excited subbands in the intrasubband relaxation processes.

As one can also see in Fig. 3(a) that for the small $d$ when $\Delta_{nF}(d) a > \hbar\omega$ and the intersubband transitions are absent, the solid, dashed, and dashed-dotted mobility curves coincide. The mobility dependence on the channel thickness $\mu(d)$, obtained by taking into consideration the excited higher-energy subbands, manifests the oscillatory behavior governed by the onset of the intersubband electron transitions with the absorption of an optical phonon. Since the intensive intrasubband transitions suppress the mobility oscillations, the mobility oscillations are stronger for the heterostructures with the low electron densities and intermediate values of the channel thickness when the excited electron levels are not occupied.

One should note here that the absolute value of the mobility calculated using the relaxation time approximation (instead of the kinetic relaxation time as in our model [Eqs. (1) and (2)] is usually smaller. In the relaxation time approximation[9–11,24,25] the electron scattering back to the initial states is not taken into account. To verify our approach, we calculated the electron mobility using the conventional relaxation time approximation for the electron density $N_s = 10^{13}$ cm$^{-2}$. The obtained result was 20%–25% smaller than the value calculated using the kinetic relaxation time approximation, which is shown in Fig. 3(a) with the solid line. In Fig. 4, we show the mobility as a function of the channel thickness calculated with the two values of the volumetric electron concentrations, $N_v = 10^{18}$ and $10^{19}$ cm$^{-3}$, and two different temperatures. The values of the channel thickness $d$, which correspond to the maxima and minima on the mobility curves, as well as the amplitudes of the mobility oscillations are similar to the results obtained for the constant sheet electron concentration $N_s$, shown in Figs. 3(a) and 3(b).

The dependence of the electron mobility on the external perpendicular electric field applied to AlN barriers is presented in Fig. 5. The results are shown for two values of the sheet electron concentration. The orientation of the field is selected to reproduce the effect of the gate bias in the conventional transistor structure. The electric field creates the triangular potential well in the conduction channel with the quantized electron energy levels and further localized the electron wave functions. The effect of the electric field is analogous to reducing the thickness of the conduction channel. However, the energy separation of the electron levels is different. The energy of the first excited electron level $\varepsilon_2$ in the flatband potential is larger than in the triangular potential, which has the same energy $\varepsilon_1$ of the ground state electron level. The mobility curves obtained in the one-subband and multisubband approaches coincide for the large electric fields due to the fact that only the ground electron quantized level is occupied. The energy separation between the electron subbands reduces with the decreasing electric field, which leads to the onset of the intersubband transitions and the mobility reduction. The wide maximum in the mobility curve for the low electron density ($N_s = 10^{12}$ cm$^{-2}$) is explained by the strong influence of the intrasubband transitions.

Our discussion so far was limited to the effect of the optical phonons on the electron mobility. At lower temperature the confined acoustic phonons can manifest themselves through the appearance of peaks or bulges in the mobility-channel thickness dependences. We calculated the confined acoustic phonon dispersion in the given structure by solving Eq. (3) using the method described by us in details elsewhere.[20] The dispersion of a few lowest confined acous-

Downloaded 12 Oct 2007 to 138.23.166.189. Redistribution subject to AIP license or copyright, see http://jap.aip.org/jap/copyright.jsp

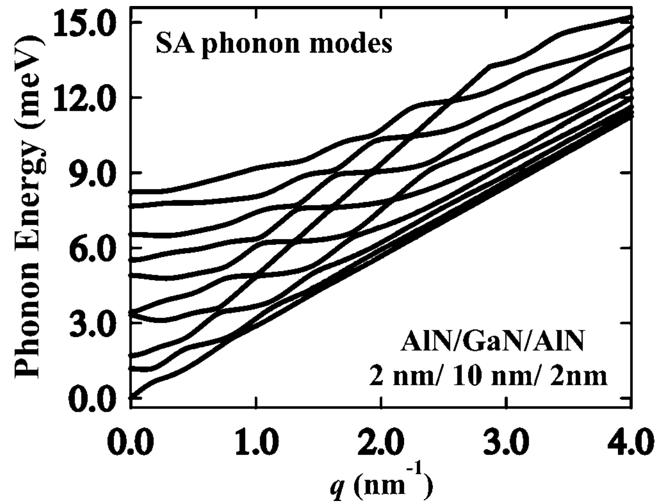


FIG. 6. Confined acoustic phonon energy dispersion for SA phonon polarization in the zinc-blende AlN/GaN/AlN heterostructure. The results are shown for a few low-energy modes in the heterostructure with the dimensions of 2 nm/10 nm/2 nm.

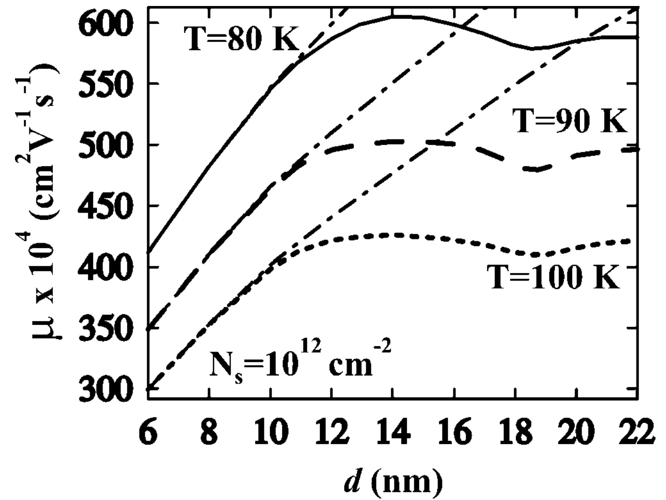


FIG. 7. Electron mobility limited by the acoustic phonons in AlN/GaN/AlN heterostructures as a function of the conduction channel thickness. The electron mobility at 80, 90, and 100 K are shown by the solid, dashed, and dotted curves, respectively.

tic phonon modes of the symmetric (SA) vibrational polarization in AlN/GaN/AlN heterostructure is shown in Fig. 6. Here we kept the nomenclature for the confined phonon mode proposed in Ref. 20. In the generic slab (without the barriers) SA modes correspond to and referred to as the dilatational phonon modes. One can see from Fig. 6 that the confined acoustic phonons have many branches and cutoff frequencies, which make them appear as "quasioptical" phonons in the low phonon energy range. Although not shown in the figure, other polarizations of the confined acoustic phonons manifest similar features.[19,20] We have calculated the confined acoustic phonons of all polarizations in order to include them in the calculation of the electron-phonon scattering. Despite the fact that the elastic continuum approximation does not give accurate results for the large values of the phonon wave vector, it is suitable for our purposes since the phonons, which interact with the electrons, are predominantly near the zone center owing to the restrictions of the momentum and energy conservation laws.[3]

After calculating the dispersion for all confined acoustic phonon branches we obtained the electron mobility from Eqs. (1) and (2). The results of calculations for the temperature range from $T=80$ to 100 K are presented in Fig. 7. The oscillations of the mobility, limited by the confined acoustic phonons, are shifted to the region of the large channel thickness in comparison with the mobility limited by the optical phonons. The latter is explained by the substantial difference between the energies of the optical and confined acoustic phonons in the considered heterostructures. The smoothing of the mobility oscillations, limited by the confined acoustic phonons, i.e., smaller amplitudes of the maxima and minima in comparison with the case of mobility limited predominantly by the optical phonons, is explained by the wider energy dispersion of the acoustic phonons. For comparison, we also show the mobility obtained by taking into account the electron ground subband only (dash-dotted curves). For the thin conduction channels ($d \leq 10$ nm) the curves obtained in the multiband and the single-band approaches coincide, while for the relatively thick channels ($d > 10$) the "single-band" mobility continues a monotonic increase and becomes much larger than the more accurate "multiband" mobility. Thus, for an accurate estimate of the electron mobility limited by the acoustic phonons, it is important to take into consideration the excited electron subbands.

## IV. CONCLUSIONS

We studied theoretically the electron mobility in AlN/GaN/AlN heterostructures with the nanometer thickness GaN conduction channels. It was found that the low-field electron mobility limited by the polar optical and confined acoustic phonons manifests oscillatory behaviors as a function of the channel thickness. The oscillations appear in the wide range of temperatures and carrier densities. It was shown that the specific mobility dependence is defined by the intersubband electronic transitions, which play an important role when the energy separation between one of the size-quantized excited electron subbands and the Fermi energy becomes comparable to the optical or confined acoustic phonon energy. The described mechanism, which is rather general and pertinent to other material systems, can be used for fine tuning the confined electron and phonon states to achieve performance enhancement of the low-power nanoscale electronic devices and improve their thermal management. It may also help in mitigating the self-heating effects, which present a major problem for GaN transistor technology.[26]

## ACKNOWLEDGMENTS

The authors acknowledge the support of the US Civil Research and Development Foundation (CRDF) through Grant No. MOE2-3057-CS-03. The work at UCR was also supported, in part, by the DARPA—SRC MARCO Center on Functional Engineered Nano Architectonics (FENA).

[1] J. Singh, *Physics of Semiconductors and Their Heterostructures* (McGraw-Hill, New York, 1992); S. M. Sze, *Physics of Semiconductor*

Downloaded 12 Oct 2007 to 138.23.166.189. Redistribution subject to AIP license or copyright, see http://jap.aip.org/jap/copyright.jsp

*Devices* (Wiley-Interscience, New York, 1982).
[2]J. Lee and M. O. Vassell, J. Phys. C **17**, 2525 (1984).
[3]V. A. Fonoberov and A. A. Balandin, Nano Lett. **6**, 2442 (2006).
[4]V. A. Fonoberov and A. A. Balandin, Nano Lett. **5**, 1920 (2005).
[5]A. A. Balandin, J. Nanosci. Nanotechnol. **5**, 7 (2005); A. A. Balandin *et al.*, Phys. Status Solidi C **11**, 2658 (2004); J. Zou *et al.*, J. Appl. Phys. **89**, 2932 (2001); A. Balandin and K. L. Wang, Phys. Rev. B **58**, 1544 (1998).
[6]K. Inoue and T. Matsuno, Phys. Rev. B **47**, 3771 (1993).
[7]T. Tsuchia and T. Ando, Phys. Rev. B **48**, 4599 (1993).
[8]X. Zianni, C. Simserides, and G. Triberis, Phys. Rev. B **55**, 16324 (1997).
[9]J. Pozhela, K. Pozhela, and V. Jucene, Fiz. Tekh. Poluprovodn. (S.-Peterburg) **34**, 1053 (2000).
[10]K. Pozhela, Fiz. Tekh. Poluprovodn. (S.-Peterburg) **35**, 1361 (2001).
[11]V. Mokerov, G. Galiev, J. Pozhela, K. Pozhela, and V. Jucene, Fiz. Tekh. Poluprovodn. (S.-Peterburg) **36**, 713 (2002).
[12]E. P. Pokatilov, D. L. Nika, and A. A. Balandin, Appl. Phys. Lett. **89**, 112110 (2006).
[13]E. P. Pokatilov, D. L. Nika, and A. A. Balandin, Appl. Phys. Lett. **89**, 113508 (2006).
[14]V. Bougrov, M. Levinshtein, S. L. Rumyantsev, and A. Zubrilov, *Properties of Advanced Semiconductor Materials: GaN, AIN, InN, BN, SiC, SiGe* (Wiley, New York, 2001), Chap. 1.
[15]B. K. Ridley, B. E. Foutz, and L. F. Eastman, Phys. Rev. B **61**, 16862 (2000).
[16]D. R. Anderson, N. A. Zakhleniuk, M. Babiker, B. K. Ridley, and C. R. Bennett, Phys. Rev. B **63**, 245313 (2001).
[17]T. Ando, A. B. Fowler, and F. Stern, Rev. Mod. Phys. **54**, 437 (1982).
[18]J. M. Ziman, *Electrons and Phonons* (Oxford University Press, Oxford, 1960), p. 421.
[19]E. P. Pokatilov, D. L. Nika, and A. A. Balandin, J. Appl. Phys. **95**, 5626 (2004).
[20]E. P. Pokatilov, D. L. Nika, and A. A. Balandin, Superlattices Microstruct. **33**, 155 (2003).
[21]J. Zi, X. Wan, G. Wei, K. Zhang, and X. Xie, J. Phys.: Condens. Matter **8**, 6323 (1996).
[22]S. M. Komirenko, K. W. Kim, M. A. Stroscio, and M. Dutta, Phys. Rev. B **59**, 5013 (1999).
[23]I. Vurgaftman and J. R. Meyer, J. Appl. Phys. **94**, 3675 (2003).
[24]S. Gokden, Phys. Status Solidi A **200**, 369 (2003).
[25]S. Gokden, R. Baran, N. Balkan, and S. Mazzucato, Physica E (Amsterdam) **24**, 249 (2004).
[26]V. O. Turin and A. A. Balandin, J. Appl. Phys. **100**, 054501 (2006); W. L. Liu, V. O. Turin, A. A. Balandin, Y. L. Chen, and K. L. Wang, MRS Internet J. Nitride Semicond. Res. **9**, 7 (2004).

**Downloaded 12 Oct 2007 to 138.23.166.189. Redistribution subject to AIP license or copyright, see http://jap.aip.org/jap/copyright.jsp**